Laser and Particle Beams (2008), *26*, 397–409. Printed in the USA.

doi:10.1017/S0263034608000414

Evolution of a high-density electron beam in the field of a super-intense laser pulse

V.V. KULAGIN,[1,*] V.A. CHEREPENIN,[2] M.S. HUR,[3] J. LEE,[1] AND H. SUK[1]

[1]APRI and School of Photon Science and Technology, GIST, Gwangju, Republic of Korea
[2]Institute of Radioengineering and Electronics RAS, Moscow, Russia
[3]Center for Advanced Accelerators, KERI, Ansan, Republic of Korea

(Received 25 March 2008; Accepted 19 May 2008)

Abstract

The evolution of a high-density electron beam in the field of a super-intense laser pulse is considered. The one-dimensional (1D) theory for the description of interaction, taking into account the space-charge forces of the beam, is developed, and exact solutions for the equations of motion of the electrons are found. It was shown that the length of the high-density electron beam increases slowly in time after initial compression of the beam by the laser pulse as opposed to the low-density electron beam case, where the length is constant on average. Also, for the high-density electron beam, the sharp peak frozen into the density distribution can appear in addition to a microbunching, which is characteristic for a low-density electron beam in a super-intense laser field. Characteristic parameters for the evolution of the electron beam are calculated by an example of a step-like envelope of the laser pulse. Comparison with 1D particle-in-cell simulations shows adequacy of the derived theory. The considered issue is very important for a special two-pulse realization of a Thomson scattering scheme, where one high-intensity laser pulse is used for acceleration, compression and microbunching of the electron beam, and the other probe counter-streaming laser pulse is used for scattering with frequency up-shifting and amplitude enhancement.

Keywords: Laser-plasma interaction; Microbunching of electron beams; Super-intense laser pulse; Ultrashort electron beams

1. INTRODUCTION

Laser generation of ultrashort particle beams is currently a topic of very intense research and has experienced much progress during recent years (Koyama *et al.*, 2006; Lifschitz *et al.*, 2006; Sakai *et al.*, 2006; Zhou *et al.*, 2007; Flippo *et al.*, 2007; Gupta & Suk 2007; Karmakar & Pukhov 2007) because such beams can be very important for many applications. For example, the ultrashort energetic electron beams can be used for injection purposes in accelerators (Umstadter *et al.*, 1996; Reitsma *et al.*, 2001), in femtosecond physics and chemistry (Barbara *et al.*, 1994; Crowell *et al.*, 2004), for generation of bright ultrashort X-ray pulses through Thomson backscattering of a probe laser pulse (Esarey *et al.*, 1993), in technological applications, and in many other fields. Besides, engineering of an ultrashort electron beam with a predefined internal structure (i.e., the beam having fast longitudinal density modulation, which is called microbunching) can be interesting for application in free-electron lasers (Marshall, 1985; Brau, 1990; Saldin *et al.*, 1999), where the microbunching is an inherent feature vitally important for functioning of the device.

Due to progress in super-intense lasers during the last decade (Danson *et al.*, 2005; Neumayer *et al.*, 2005, Zvorykin *et al.*, 2007; Kalashnikov *et al.*, 2007; Canova *et al.*, 2007), high-density electron beams with linear dimensions of 10–20 μm became available in laboratories by using table-top laser-plasma accelerators (Mangles *et al.*, 2004; Geddes *et al.*, 2004; Faure *et al.*, 2004; Hafz *et al.*, 2007). Such a high-density electron beam can be additionally accelerated, compressed, and microbunched by a field of another super-intense laser pulse to improve the properties of the electron beam (Kulagin *et al.*, 2006*a*, 2006*b*). Alternatively, ordinary electron beams can be used for acceleration, compression, and microbunching by a super-intense laser pulse. After that, these preprocessed electron beams can

Address correspondence and reprint requests to: Hyyong Suk, APRI and School of Photon Science and Technology, GIST, Gwangju 500-712, Republic of Korea. E-mail: hysuk@gist.ac.kr
*E-mail: victorvkulagin@yandex.ru; On leave from Sternberg Astronomical Institute of Moscow State Univesity, Russia.

be effectively utilized, e.g., for Thomson backscattering of a probe counter-streaming laser pulse with frequency up-shifting and amplitude enhancement (Cherepenin & Kulagin, 2004; Kulagin *et al.*, 2004*a*, 2004*b*). These two-pulse methods allow in principle to control all parameters of the converted electromagnetic pulse in a full extent (duration, frequency, shape of an envelope, carrier-envelope phase, etc.) in contrast with the case of one-pulse method of over critical plasma excitation (Baeva *et al.*, 2007), or with the case of free electron lasers (Saldin *et al.*, 2008), where it is not easy to change these parameters. In the two-pulse generation scheme, coherent properties of the electron beam directly influence the statistics of the generated high-frequency radiation. Therefore, an investigation of the dynamic behavior of the dense electron beam in the field of a high-intensity laser pulse is a very important issue, and we address it in this paper.

Having in mind the above mentioned application for the dense electron beam, one can define the differences of our problem from the usual study of the electron beams: high density of the beam, large energy spread of the electrons (sometimes reaching 100%), relatively short (with respect to the ordinary electron beams) propagation distance, for which the parameters of the electron beam should be calculated (for backscattering, the evolution time of the beam on the order of 0.3–0.5 ps is more than enough so that the required maximal propagation distance of the beam is less than 0.15 mm), and last, permanent action of an ultrastrong electromagnetic wave on the electron beam during evolution. Therefore, several analytic and numeric algorithms (Reiser, 1994; Lapostolle *et al.*, 1996; Wangler, 1998; Fubiani *et al.*, 2006) used so far for description of the electron beam evolution in the presence of the space-charge forces can be hardly applied to our case.

For a dense electron beam interacting with an ultraintense laser pulse, two extreme cases are possible. In the first case (case 1 below), the electromagnetic wave gives only small modification to the dynamics of the electron beam evolving under the space-charge forces. In the second case (case 2), which is considered below in details, the space-charge forces can be considered as a small perturbation (at least, within some initial interval of time) to the electron beam dynamics in the field of an ultraintense electromagnetic wave. The limiting situation of this second case, when space-charge forces and radiation of the electrons can be entirely omitted, was considered earlier (Kulagin *et al.*, 2006*a*; Kulagin *et al.*, 2006*b*), and the solutions for the electron motion in a given laser field were utilized to study the evolution of low-density electron beams in the field of ultraintense laser pulses. It was shown that the laser pulse front compresses and accelerates the electron beam, and induces a density wave inside the beam producing characteristic microbunching. This spatial structure can be supported without change during all time of interaction. However, it is not evident beforehand, what value of the electron density for the electron beam with a certain initial length can be considered as low in our particular problem, besides, if the density is not low, then how will the dynamics of the electrons in a laser field be modified by the space-charge forces of the electron beam, and what new effects can arise? In this paper, the answers to these questions are presented.

The paper is organized as follows: the one-dimensional (1D) mathematical model with equations of motion for the electrons and exact analytical solutions to these equations are specified in Section 2. In Section 3, the characteristic parameters for the evolution of the high-density electron beam are investigated by an example of the laser pulse with a step-like envelope acting on the initially nonrelativistic electron beam. The analytical expression for the length of the electron beam as a function of time is derived. Taking into account the space-charge forces in the high-density electron beam results in a slow longitudinal spreading of the beam with corresponding decrease of an average electron density. However, the microbunching is still present here, and during the evolution, the total number of humps in the beam increases. In Section 4, the analytical expression for the longitudinal density profile of the electron beam as a function of time is derived and compared with the results of the 1D particle-in-cell (PIC) simulations showing good agreement. Also here, the other difference from the vanishingly low electron beam density case is revealed: it is the presence of a very short and very high frozen density peak in the front side of the electron beam (side illuminated with the laser pulse), which originates from the modulation of initial counter-velocities of the electrons that are accelerated by the space-charge forces. In Section 5, discussion of the results is presented and conclusions are derived.

2. MATHEMATICAL MODEL AND EQUATIONS OF MOTION FOR THE ELECTRONS

For description of the interaction of an intense laser pulse with an electron beam, a 1D model is used below. Formally, this model can be applicable in cases, where all variables depend only on one coordinate and time, i.e., diameters of laser and electron beams are infinite. In reality, 1D model can also be useful for a quasi-1D character of interaction of a laser pulse with an electron beam, when variables change along the transverse coordinates much slowly than along the longitudinal coordinate. For this case, a laser spot size and an electron beam diameter should be much larger than longitudinal (along the laser beam axis) dimensions of the electron medium (for example, this situation is realized quite well in laser pulse interaction with solid nanofilms (Kulagin *et al.*, 2007*a*); for high-density electron beams from laser-plasma accelerators, the requirement for quasi-1D character of interaction can be fulfilled if the laser spot is larger than 20–30 μm).

The laser pulse is modeled below by a plane electromagnetic wave with amplitude E_0, frequency ω, and wave vector $\mathbf{k}(k = \omega/c)$, which is running along the z axis and is linearly

https://doi.org/10.1017/S0263034608000414 Published online by Cambridge University Press

polarized with only $E_y = E_0 e_y$ non-zero component. The electron beam is modeled by a set of parallel electron sheets (ESs) each labeled by its initial position Z_{0e} (Lagrangian description). Each ES has infinite dimensions in x- and y-directions, besides, the motion of the ESs is assumed to be plane-parallel (one of the ESs is shown in Fig. 1).

Let us first consider only one ES. Charge and current densities for it are $\rho(z, t) = \sigma\delta[z - Z(t)]$ and $\mathbf{j}(z, t) = \sigma\mathbf{v}(t)\delta[z - Z(t)]$, where σ is the surface charge density, $\mathbf{v}$ and Z are the velocity and the coordinate of the ES. Then, formal solutions to the Maxwell's equations for the fields of the ES at coordinate z and time t can be obtained with the help of Green function and have the form (Il'in *et al.*, 1999; Kulagin *et al.*, 2004*b*; Kulagin *et al.*, 2007*b*)

$$\begin{aligned} E_{ze}(z, t) &= 2\pi\sigma \operatorname{sign}[z - Z(t')], \\ \mathbf{E}_{\perp e}(z, t) &= -2\pi\sigma \frac{\vec{\beta}_\perp(t')}{1 - \beta_z(t') \operatorname{sign}[z - Z(t')]}, \\ \mathbf{H}_e(z, t) &= \frac{2\pi\sigma \operatorname{sign}[z - Z(t')][\vec{\beta}_\perp(t') \times \mathbf{e}_z]}{1 - \beta_z(t') \operatorname{sign}[z - Z(t')]}, \end{aligned} \tag{1}$$

where $\vec{\beta} = \mathbf{v}/c$, c is the velocity of light in vacuum, $\mathbf{E}_{\perp e} = E_{xe}\mathbf{e}_x + E_{ye}\mathbf{e}_y$, $\mathbf{v}_\perp = v_x\mathbf{e}_x + v_y\mathbf{e}_y$, and t' is the retarded time

$$c(t - t') = |z - Z(t')|. \tag{2}$$

Eq. (1) describe the field of an infinite ES, in which case the field components E_{ze} and $\mathbf{E}_{\perp e}$ can be interpreted as the longitudinal (Coulomb) field and the radiation field of the sheet, respectively.

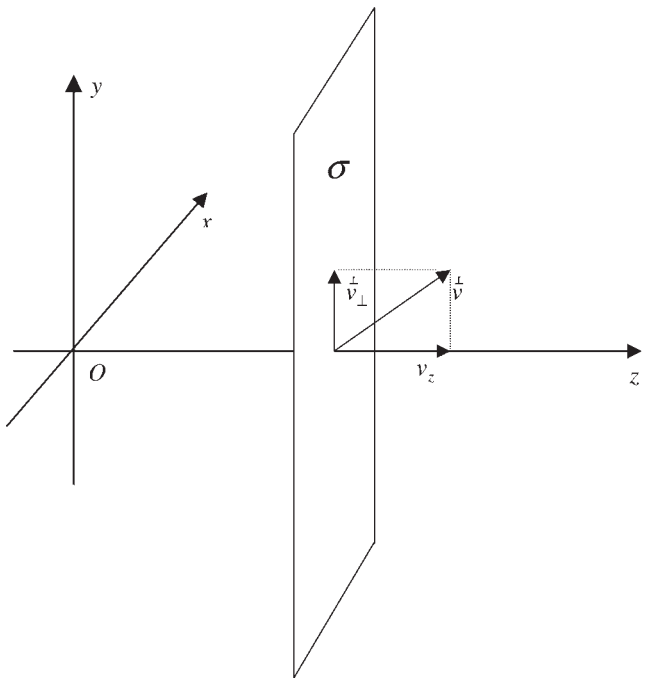

Fig. 1. Geometry of the model.

The total fields of the electron beam can be considered as the sum of the fields of all ESs calculated in accordance with Eqs. (1) and (2) with proper time and space variables. In a general case, the total field can be calculated only numerically (Kulagin *et al.*, 2007*b*). However, if the longitudinal dimension of the electron beam after compression (Kulagin *et al.*, 2006*a*; 2006*b*) is not very small (not less than the laser wavelength), a coherent part of the electron beam radiation in the laser field greatly reduces (Kulagin *et al.*, 2007*b*), and the radiation reaction force due to $\mathbf{E}_{\perp e}$ can be omitted in the model. This condition is fulfilled if the laser amplitude is not very high to compress the initial electron beam into a bunch with the length much smaller than the laser wavelength. Therefore, only static Coulomb forces due to E_{ze} can be accounted for in the model (we will call this a Coulomb interaction below). For initially very thin targets such as foils, this approximation is not valid, and both components of the field for the ESs should be considered (Cherepenin & Kulagin, 2004; Kulagin *et al.*, 2004*b*).

When calculating the Coulomb interaction between the ESs below, we suppose that there are no intersections of trajectories $Z(t)$ of the ESs (none of the ESs overtakes the other ES, and the numbers of the ESs on the left and the right sides of a particular ES are constants in time). Then, the Coulomb force between each ES and other ESs can also be considered as constant in time. The equations of motion for the electrons, which belong to the ES with initial coordinate Z_{0e}, have the following form:

$$\begin{aligned} \frac{dp_y}{dt} &= eE_y\left(1 - \frac{p_z}{mc\gamma}\right), \\ \frac{dp_z}{dt} &= \frac{eE_y p_y}{mc\gamma} + 2\pi n_0 e^2(2Z_{0e} - l), \\ \frac{d\gamma}{dt} &= \frac{eE_y p_y}{m^2c^2\gamma} + 2\pi n_0 e^2(2Z_{0e} - l)\frac{p_z}{m^2c^2\gamma}, \\ \frac{dZ}{dt} &= \frac{p_z}{m\gamma}, \end{aligned} \tag{3}$$

where p_y and p_z are the transversal and the longitudinal momenta of the electron, e and m are the charge and the rest mass of an electron, n_0 and l are the initial density and the initial length of the electron beam, and $\gamma^2 = 1 + p_y^2/(mc)^2 + p_z^2/(mc)^2$. In Eq. (3), we suppose that initial coordinate for the left end of the electron beam is $Z_{0e} = 0$ and, for the right end, it is $Z_{0e} = l$ (other configurations can be considered on the similar basis).

Below, it is convenient to use normalized momenta $p_y/(mc) \to p_y$ and $p_z/(mc) \to p_z$. When the density of the electron beam is vanishing, $n_0 \to 0$, and the field of an electromagnetic wave is the only present, the value

$$\kappa(t) = \gamma(t) - p_z(t) \tag{4}$$

is invariant and is equal to unity for the electrons with the zero initial momenta (Landau & Lifshitz, 1975). In our case, the Coulomb forces are also present in the model,

https://doi.org/10.1017/S0263034608000414 Published online by Cambridge University Press

however, as we supposed, they give only some correction to the motion of the electrons in the ultraintense electromagnetic wave (cf. case 2 of the Introduction) so again it is convenient to transfer to the variable κ, which will be a slowly varying variable, instead of γ and p_z, whose variations are fast. Then, introducing a new independent variable

$$\theta(Z_{0e}, t) = \omega t - kZ(Z_{0e}, t), \tag{5}$$

which is different for the different ESs, one has the following equations of motion for the electrons with the initial coordinate Z_{0e}

$$\begin{aligned} \frac{dp_y}{d\theta} &= -a_0 e_y(\theta), \\ \frac{d\kappa}{d\theta} &= \nu(kl - 2kZ_{0e}), \\ \frac{d(kZ)}{d\theta} &= \frac{1+p_y^2}{2\kappa^2} - \frac{1}{2}, \end{aligned} \tag{6}$$

where $a_0 = |e|E_0/(mc\omega)$, $\nu = \omega_p^2/(2\omega^2) = n_0 r_e \lambda^2/(2\pi)$, $\omega_p = \sqrt{4\pi n_0 e^2/m}$ is the characteristic plasma frequency, r_e and λ are the classical radius of an electron and the laser wavelength correspondingly. Also, the variable γ and the longitudinal momentum p_z can be defined from the usual expressions

$$\begin{aligned} \gamma &= (1 + p_y^2 + \kappa^2)/(2\kappa), \\ p_z &= (1 + p_y^2 - \kappa^2)/(2\kappa). \end{aligned} \tag{7}$$

General solutions to Eqs. (3) and (6) have the following parametric form

$$\begin{aligned} p_y(\theta) &= p_{y0} - \int_{\theta_0}^{\theta} a_0(\theta') e_y(\theta') d\theta', \\ \kappa(\theta) &= \kappa_0 + \nu(kl - 2kZ_{0e})\theta, \\ kZ(\theta) &= kZ_{0e} + \int_{\theta_0}^{\theta} [1 + p_y^2(\theta')] d\theta' / [2\kappa^2(\theta')] - \theta/2, \\ \omega t &= \theta + kZ(\theta), \end{aligned} \tag{8}$$

where $\theta_0 = \omega t_0 - kZ_{0e}$, p_{y0} and κ_0 are the initial values at the initial moment of time $t = t_0$ for the transversal momentum p_y and the parameter κ, which depend on the initial position Z_{0e} of the electron and can be different for the electrons belonging to the different ESs.

From Eqs. (6) and (8), one can conclude that the motion of the central ES with the coordinate $Z_{0e} = l/2$ have no perturbation due to the Coulomb forces, so this ES is moving just as in the given field of the electromagnetic wave only, and $\kappa(\theta) = \kappa_0$. Besides, the outermost ESs feel the maximal Coulomb force, which is defined by all electrons in the electron beam and is proportional to a parameter α (Vshivkov *et al.*, 1998; Kulagin *et al.*, 2004*b*)

$$\alpha = \nu kl = \pi \frac{\omega_p^2}{\omega^2} \frac{l}{\lambda}. \tag{9}$$

The parameter κ for the most left electrons is increasing with θ according to equation $\kappa_l = \kappa_{l0} + \alpha\theta$, and, for the most right electrons, it is decreasing, $\kappa_r = \kappa_{r0} - \alpha\theta$. For the first glance, for some value of θ, the parameter κ_r can become equal to zero, giving the divergence for p_z and γ. However, it can be verified that this value of θ cannot be achieved for any finite time t.

General solutions (8) are valid for both cases 1 and 2 considered in the Introduction. The electron momentum p_y has a period $\theta_p = 2\pi$. If, during this time, a change in κ is small enough, i.e., $2\pi\alpha \ll \kappa_0$ then the Coulomb forces give only some perturbation for the dynamics of the electron beam in the given external electromagnetic wave, and case 2 is realized. In the opposite situation, the dynamics of the electrons will be defined primarily by the Coulomb forces (case 1 in the Introduction). It is necessary to note, that parameter α depends not only on the density n_0 of the electron beam, but on the total length (l) of the beam also, so even in a long low-density electron beam, the Coulomb forces can be important (this conclusion is true if the 1D model is applicable, i.e., the diameter of the beam is considerably larger than its length). Below, only case 2 with $2\pi\alpha \ll \kappa_0$ will be considered. For $\kappa_0 \simeq 1$ and $l = 10$ μm, this condition corresponds to $\nu \ll 2.5 \times 10^{-3}$ and $n_0 \ll 5.5 \cdot 10^{18} \mathrm{cm}^{-3}$.

3. CHARACTERISTIC PARAMETERS OF THE ELECTRON BEAM EVOLUTION FOR THE STEP-LIKE ENVELOPE OF THE LASER PULSE

3.1. Solutions for Equations of Motion for Initially Nonrelativistic Electron Beam

To study the characteristics of a dense electron beam evolution and to demonstrate the capabilities of the theory, it is useful to consider one of the simplest form for the laser pulse envelope, e.g., a step-like envelope, where the integral for p_y can be calculated analytically (smooth envelope cases can be considered on the similar basis using Eq. (8)). Also, we will suppose initially nonrelativistic electron beam, which most prominently demonstrates the peculiarities of the evolution of the dense electron beam in the super-intense laser field (non-zero initial momenta for p_y and p_x lead only to the changes in numbers due to electron mass scaling and leave the qualitative results intact). Let us assume that the front of the laser beam touches the electron beam at point $Z_{0e} = 0$ when $\omega t = 0$. Then, the laser field is $E_y(\theta) = E_0 \sin\theta$ for $\theta \geq 0$ and zero for $\theta < 0$, and for the transversal momentum p_y, one has for $\theta \geq 0$ from Eq. (8)

$$p_y(\theta) = a_0(\cos\theta - 1), \tag{10}$$

https://doi.org/10.1017/S0263034608000414 Published online by Cambridge University Press

and $p_y = 0$ for $\theta < 0$, if the zero initial value is supposed for p_y. It is convenient to consider the evolution of the electron beam in two intervals, $\theta < 0$ and $\theta > 0$, separately. Laser pulse need some time to reach the ES with the initial coordinate Z_{0e}. During this time, this ES will move due to the space-charge (static Coulomb) forces, so when the laser pulse reaches it, this ES will have the following parameters of motion, which are the solutions of Eq. (3) with the zero amplitude of the electromagnetic field

$$\begin{aligned} kZ_{in} &= kZ_{0e}\{1 + [1 + \nu(kl - 2kZ_{0e})kZ_{0e}]^{-1}\}/2, \\ \kappa_{in} &= \sqrt{1 + [\nu(kl - 2kZ_{0e})kZ_{in}]^2} \\ &\quad + \nu(kl - 2kZ_{0e})kZ_{in} = 1 + \nu(kl - 2kZ_{0e})kZ_{0e}, \end{aligned} \tag{11}$$

where $\alpha kl < 1$, and zero value for the initial longitudinal momentum p_z is supposed ($\kappa_0 = 1$). The values κ_{in} and kZ_{in} are just the initial values for the evolution of the electron beam in the field of the laser pulse, and with this values as initial, the parameter θ_0 in Eq. (8) should be considered as zero. Then, equation for the coordinate Z can be split into two equations for slow Z_s and fast Z_f parts according to the formulas

$$\begin{aligned} \frac{d(kZ_s)}{d\theta} &= \frac{1 + 3a_0^2/2}{2[\kappa_{in} + \nu(kl - 2kZ_{0e})\theta]^2} - \frac{1}{2}, \\ \frac{d(kZ_f)}{d\theta} &= a_0^2 \frac{\cos 2\theta - 4\cos\theta}{4[\kappa_{in} + \nu(kl - 2kZ_{0e})\theta]^2} \end{aligned} \tag{12}$$

with correspondent solutions

$$\begin{aligned} kZ_s &= kZ_{in} + \frac{(1 + 3a_0^2/2)\theta}{2\kappa_{in}[\kappa_{in} + \nu(kl - 2kZ_{0e})\theta]} - \frac{\theta}{2}, \\ kZ_f &= a_0^2 \frac{\sin 2\theta - 8\sin\theta}{8[\kappa_{in} + \nu(kl - 2kZ_{0e})\theta]^2} \\ &\quad + a_0^2\nu(kl - 2kZ_{0e}) \frac{1 - \cos 2\theta + 16(\cos\theta - 1)}{8[\kappa_{in} + \nu(kl - 2kZ_{0e})\theta]^3}, \end{aligned} \tag{13}$$

where the solution for Z_f is correct up to the first order in $\nu(kl - 2kZ_{0e})$ (cf. $2\pi\alpha = 2\pi\nu kl \ll \kappa_0$ and $\kappa_{in} \approx \kappa_0 = 1$).

From Eq. (13), one can conclude that $|Z_f| \ll Z_s$ for not very small values of θ. Then, the slow evolution of the electron beam can be evaluated only using Z_s, and the transition from parameter θ to the time ωt becomes simple

$$\omega t = kZ_{in} + \frac{\theta}{2}\left[1 + \frac{(1 + 3a_0^2/2)}{\kappa_{in}(\kappa_{in} + \nu(kl - 2kZ_{0e})\theta)}\right]. \tag{14}$$

From the first equation of the system (12), one can conclude that the coordinate of the electron with the initial coordinate $Z_{0e} \geq l/2$ will increase infinitely, while the electrons with the initial coordinates $Z_{0e} < l/2$ will turn back at point

$$\theta_{tb} = \frac{\sqrt{1 + 3a_0^2/2} - \kappa_{in}}{\nu(kl - 2kZ_{0e})}, \tag{15}$$

or, for laboratory time,

$$\omega t_{tb} = kZ_{in} + \frac{1 - \kappa_{in}^2 + 3a_0^2/2}{2\kappa_{in}\nu(kl - 2kZ_{0e})}. \tag{16}$$

At this moment, the coordinate Z will have the value

$$kZ_{tb} = kZ_{in} + \frac{(\sqrt{1 + 3a_0^2/2} - \kappa_{in})^2}{2\kappa_{in}\nu(kl - 2kZ_{0e})}, \tag{17}$$

and, for $a_0 \gg 1$ supposed below, it is about $kZ_{in} + 3a_0^2/[4\kappa_{in}\nu(kl - 2kZ_{0e})]$. So the most left ES ($Z_{in} = Z_{0e} = 0$, $\kappa_{in} = 1$) will turn first at

$$\begin{aligned} \theta_{ce} &= \frac{\sqrt{1 + 3a_0^2/2} - 1}{\alpha} \simeq \frac{a_0}{\alpha}\sqrt{\frac{3}{2}}, \\ \omega t_{ce} &= \frac{3a_0^2}{4\alpha}, \end{aligned} \tag{18}$$

and this value of ωt can be considered as a time of coherent evolution for the beam. Actually, after the turning of the most left ES, electrons in the beam will move away with relativistic velocity so the total beam cannot be considered as a single whole (however, major part of the ESs continues to move relativistically at this time, so a truncated electron beam can still be used). The maximal coordinate of the most left ES is

$$kZ_{lmax} = \frac{(\sqrt{1 + 3a_0^2/2} - 1)^2}{2\alpha} \simeq \frac{3a_0^2}{4\alpha}. \tag{19}$$

Also, the most left ES returns to its initial point with the coordinate $Z_0 = 0$ at the moment

$$\theta_r = \omega t_r = \frac{3a_0^2}{2\alpha}. \tag{20}$$

For the vanishingly small density of the electron beam, none of the ESs will return to the initial position.

3.2. Analysis of the Motion for the ESs

The motion of the ESs in the laser fields with large amplitudes consists of two parts (cf. Fig. 2): a long period of forward longitudinal movement with a relativistic velocity and a short period of movement with a small velocity in forward (for the right ESs) or in backward (for the left ESs) directions. During this short interval, the ES switches from one cycle of the laser field to the other. For $n_0 \to 0$, the period of time between two successive switches, which is determined by successive vanishing of p_y, i.e., for $\theta_n = 2\pi n$ and $\theta_{n+1} = 2\pi(n + 1)$, does not depend on time and initial coordinate of the ES, and is equal to (Kulagin *et al.*, 2006*a*)

$$\omega T_{sw} = 2\pi(1 + 3a_0^2/4). \tag{21}$$

https://doi.org/10.1017/S0263034608000414 Published online by Cambridge University Press

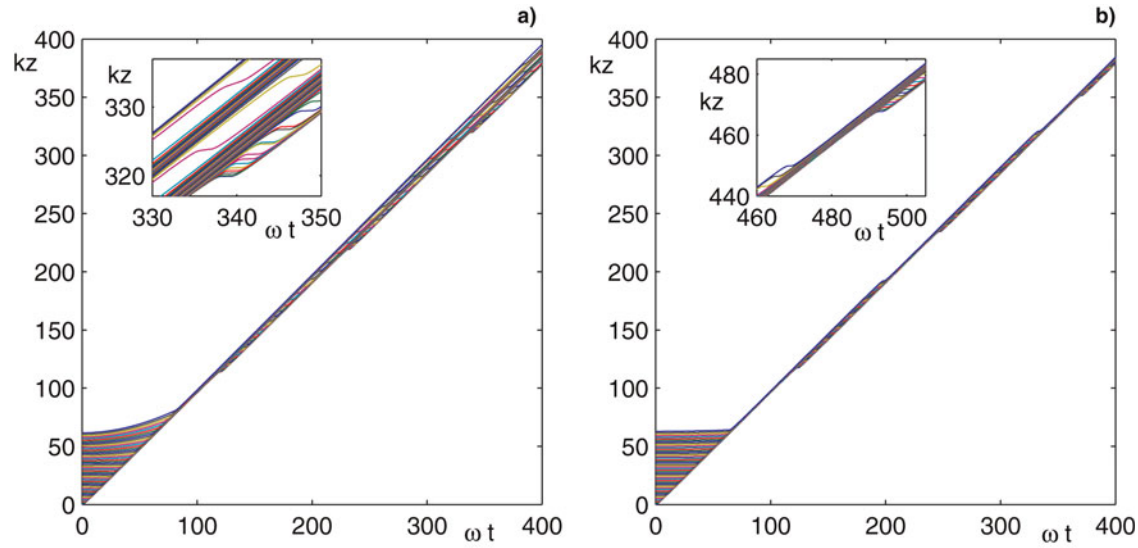

Fig. 2. (Color online) Trajectories of some ESs of the electron beam in the field of a super-intense laser pulse with the step-like envelope ($a_0 = 5$): (**a**) $\nu = 10^{-4}$ and $n_0 = 2.2 \times 10^{17}$ cm^{-3}, (**b**) $\nu = 10^{-5}$ and $n_0 = 2.2 \times 10^{16}$ cm^{-3}. In the insets, the zoomed views of the trajectories are shown: (a) multilayer structure of the beam and the third switching of the left ESs; (b) monolayer configuration of the beam (from $\omega t \simeq 470$ to $\omega t \simeq 490$) and switchings—third for the right ESs (below $\omega t \simeq 470$) and forth for the left ESs (above $\omega t \simeq 490$).

Hence, the most left and the most right ESs in the electron beam with vanishingly small density switch within one cycle of the laser field, so the length of the electron beam does not grow in average. For the dense electron beam, this period depends on time. Moreover, T_{sw} depends also on the initial coordinate Z_{0e}: it grows for the ESs with the initial coordinates $Z_{0e} > l/2$ and decreases for the ESs with $Z_{0e} < l/2$. For $Z_{0e} = l/2$, this period is constant and is determined by Eq. (21). So, the length of the high-density electron beam will grow in average. Actually, from Eq. (14), one has for the times of switching for the most right and the most left ESs

$$\omega t_{swr} = kZ_{inr} + \frac{\theta_n}{2} + \frac{\theta_n(1 + 3a_0^2/2)}{2\kappa_{inr}(\kappa_{inr} - \alpha\theta_n)},$$
$$\omega t_{swl} = \frac{\theta_n}{2} + \frac{\theta_n(1 + 3a_0^2/2)}{2(1 + \alpha\theta_n)}, \tag{22}$$

where one has now from Eq. (11) for the coordinate Z_{inr} and the parameter κ_{inr}:

$$kZ_{inr} = kl[1 + (1 - \alpha kl)^{-1}]/2,$$
$$\kappa_{inr} = 1 - \alpha kl. \tag{23}$$

Depending on the values of ωt_{swr} and ωt_{swl}, the electron beam can exist either in a single layer (only one hump in the density distribution along z) or multilayer configurations. When the multilayer configuration is realized, the number of full layers in the electron beam at time ωt can be defined as the difference between the numbers of the switchings for the most left and for the most right ESs, which is given by the whole part of the value

$$N_l = \frac{\theta_l}{2\pi} - \frac{\theta_r}{2\pi}, \tag{24}$$

where θ_r and θ_l are the corresponding values of θ for the most right and the most left ESs (we suppose that the front of the laser pulse already reached the most right ES, and all ESs are in motion, $\omega t \geq kZ_{inr}$):

$$\omega t = kZ_{inr} + \frac{\theta_r}{2} + \frac{\theta_r(1 + 3a_0^2/2)}{2\kappa_{inr}(\kappa_{inr} - \alpha\theta_r)},$$
$$\omega t = \frac{\theta_l}{2} + \frac{\theta_l(1 + 3a_0^2/2)}{2(1 + \alpha\theta_l)}. \tag{25}$$

Then, for θ_r and θ_l, one has quadratic equations with the following solutions:

$$\theta_r = \frac{4\kappa_{inr}^2(\omega t - kZ_{inr})}{D + \sqrt{D^2 - 8\kappa_{inr}^3\alpha(\omega t - kZ_{inr})}},$$
$$D = 1 + 3a_0^2/2 + \kappa_{inr}^2 + 2\kappa_{inr}\alpha(\omega t - kZ_{inr}),$$
$$\theta_l = \frac{2\omega t}{E + \sqrt{E^2 + 2\alpha\omega t}},$$
$$E = 1 + 3a_0^2/4 - \alpha\omega t. \tag{26}$$

The length of the electron beam at time t is defined as $l_b(t) = Z_r(t) - Z_l(t) = Z_r[\theta_r(t)] - Z_l[\theta_l(t)]$. Then from Eq. (5), one has

$$l_b(t) = \frac{\theta_l(t) - \theta_r(t)}{2\pi}\lambda = N_l(t)\lambda. \tag{27}$$

https://doi.org/10.1017/S0263034608000414 Published online by Cambridge University Press

So the electron beam in the strong electromagnetic wave can be imagined as a set of N_l layers each having the same full length equal to λ (may be, barring the boundary layers), and this length does not depend on time and the initial coordinate Z_{0e}. Actually, such a structure in space is defined by the electromagnetic wave itself, for which every two neighboring maxima or minima are separated just by the same distance λ.

For not very large time ωt long before the turning of the most left ES ($2\alpha\omega t \ll 3a_0^2/2$, cf. Eqs. (18)), the length of the electron beam can be estimated from Eq. (26) as

$$kl_b(t) = \frac{kZ_{inr}}{1+3a_0^2/4}\left(1+\frac{2\alpha\kappa_{inr}(\omega t - kZ_{inr})}{1+\kappa_{inr}^2/(1+3a_0^2/2)}\right) + \frac{\alpha(\omega t)^2}{(1+3a_0^2/4)^2} + \frac{4\alpha\kappa_{inr}^3(\omega t - kZ_{inr})^2}{(1+3a_0^2/2+\kappa_{inr}^2)^2}. \quad (28)$$

So for $\omega t \gtrsim kZ_{inr}$, the initial compression of the electron beam is defined by very similar formula as for $\alpha = 0$ case (Kulagin *et al.*, 2006*a*), however, the equivalent initial thickness of the beam now is Z_{inr}, which is greater than Z_{0e} due to the action of the static Coulomb forces. For the vanishing density of the electron beam, $Z_{inr} = Z_{0e}$ and Eq. (28) gives exactly the same value for the length of the beam as in the paper by Kulagin *et al.* (2006*a*).

The single-layer configuration after the nth switching is possible if $\omega t_{swl}(\theta_{n+1}) > \omega t_{swr}(\theta_n)$, which gives the following condition for n

$$An^2 + Bn + C < 0, \quad (29)$$

where the coefficients A, B, and C are the following

$$A = 2\pi\alpha[(1+3a_0^2/2)(1+\kappa_{inr}) - 2\pi\alpha\kappa_{inr}(kZ_{inr}/\pi - 1)],$$
$$B = (1-\kappa_{inr}+2\pi\alpha)[(1+3a_0^2/2)(1+\kappa_{inr}) - 2\pi\alpha\kappa_{inr}(kZ_{inr}/\pi - 1)],$$
$$C = \kappa_{inr}^2[(kZ_{inr}/\pi - 1)(1+2\pi\alpha) - 1 - 3a_0^2/2]. \quad (30)$$

Realization of the single-layer configuration after the nth switching requires at least an existence of the single-layer configuration after the initial compression of the electron beam. Then, one has (Kulagin *et al.*, 2006*a*) $kZ_{inr} < 2\pi(1+3a_0^2/4)$, and the coefficient C is negative, while A and B are positive. Then, for the maximal value of n, one has

$$n = \left[(\sqrt{B^2 - 4AC} - B)/(2A)\right], \quad (31)$$

and $[x]$ means the whole part of x.

In Figure 2, the evolutions of the beams with $l = 10$ μm and $\nu = 10^{-4}$ (a) or $\nu = 10^{-5}$ (b) are presented (laser amplitude is $a_0 = 5$, laser wavelength is $\lambda = 1$ μm). The initial electron density for the $\nu = 10^{-4}$ case is $n_0 = 2.2\times10^{17}$ cm^{-3}, and for the $\nu = 10^{-5}$ case, it is $n_0 = 2.2\times10^{16}$ cm^{-3}. The trajectories of the ESs in Figure 2 were calculated with the help of 1D MATLAB code EXACT (Cherepenin *et al.*, 2001; Kulagin *et al.*, 2004*b*, 2007*b*), which uses the exact expressions for the electromagnetic fields of the ESs and takes into account self-consistently the radiation of the electron beam. Also, the crossings of the trajectories are allowed in the code. In Figure 2a, the increase due to the static Coulomb forces of the coordinate of the right ESs before interaction with the laser pulse is evident (from $kZ_{0e} \simeq 63$ to $kZ_{in} = 84$ for the most right ESs). For the smaller beam density $\nu = 10^{-5}$, the single-layer configuration still exists after the forth switching of the ESs; for $\nu = 10^{-4}$, it disappears after the first switching, and the single-layer configuration exists here only after the primary compression of the electron beam (from $\omega t \simeq 84$ to $\omega t \simeq 120$). In the inset of Figure 2a, the multilayer structure of the beam and the third switching of the left ESs are shown. In the inset of Figure 2b, the single-layer configuration of the beam after the third switching is shown (from $\omega t \simeq 470$ to $\omega t \simeq 490$), and also, third switching for the right ESs (below $\omega t \simeq 470$) and forth switching for the left ESs (above $\omega t \simeq 490$).

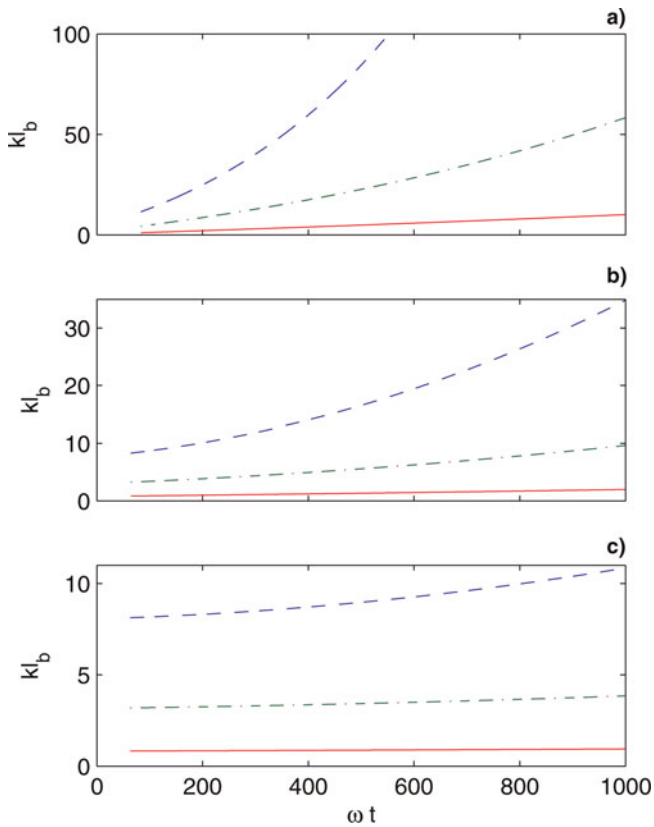

Fig. 3. (Color online) The length of the high-density electron beam (with initial length of 10 μm) as a function of time in the field of a super-intense laser pulse with the step-like envelope: (**a**) $\nu = 10^{-4}$ ($n_0 = 2.2\times10^{17}$ cm^{-3}), (**b**) $\nu = 10^{-5}$ ($n_0 = 2.2\times10^{16}$ cm^{-3}), (**c**) $\nu = 10^{-6}$ ($n_0 = 2.2\cdot10^{15}$ cm^{-3}). Solid lines (red online) is for $a_0 = 10$, dash-dotted lines (green online) is for $a_0 = 5$, and dashed lines (blue online) is for $a_0 = 3$.

https://doi.org/10.1017/S0263034608000414 Published online by Cambridge University Press

All these switching times, numbers of layers and lengths of the electron beam coincide rather well with the analytic predictions from Eqs. (22)–(31).

In Figure 3, the lengths of the electron beam as a functions of time, which are calculated from Eq. (27), are presented for different laser pulse amplitudes a_0 and initial electron beam densities n_0 (the initial length of the electron beam is 10 μm). From these figures, one can conclude that, if the time of evolution is not too large (less than 1 ps), the electron beam with the initial density $n_0 < 10^{15}$ cm^{-3} can be considered as a low-density beam in the fields of laser pulses with amplitudes $a_0 > 3$.

4. DENSITY DISTRIBUTION FOR THE DENSE ELECTRON BEAM

4.1. Analytical Expression for the Density Distribution of the Electron Beam

Let us now derive analytically the density distribution for the electron beam. For the constant initial density n_0 of the beam, one has, taking the conservation of charge into account

$$n(Z_{0e}, t) = n_0 \left\{ \frac{d[kZ(Z_{0e}, t)]}{d(kZ_{0e})} \right\}^{-1}. \tag{32}$$

In our case, the coordinate Z of some ES depends on its initial coordinate Z_{0e} directly and, also, through the dependence of θ on Z_{0e}. So one has

$$\frac{d[kZ(Z_{0e}, t)]}{d(kZ_{0e})} = \left\{ \frac{\partial[kZ(Z_{0e}, \theta)]}{\partial(kZ_{0e})} + \frac{\partial[kZ(Z_{0e}, \theta)]}{\partial\theta} \cdot \frac{\partial\theta}{\partial(kZ_{0e})} \right\}_{\theta=\theta(Z_{0e},t)}. \tag{33}$$

Expression for $\partial[kZ(Z_{0e}, \theta)]/\partial\theta$ can be defined from Eq. (6), and $\partial\theta/\partial(kZ_{0e})$ can be evaluated from Eq. (5) with the help of the rule for the differentiation of implicit functions. Then, one has

$$\frac{d[kZ(Z_{0e}, t)]}{d(kZ_{0e})} = \left\{ \frac{\partial[kZ(Z_{0e}, \theta)]}{\partial(kZ_{0e})} \cdot \frac{\kappa(Z_{0e}, \theta)}{\gamma(Z_{0e}, \theta)} \right\}_{\theta=\theta(Z_{0e},t)}. \tag{34}$$

Partial derivative $\partial[kZ(Z_{0e}, \theta)]/\partial(kZ_{0e})$ can be evaluated either from Eq. (8) using the rules for the differentiation of integrals depending on parameters, or, alternatively, directly from Eq. (13) (which will be different for different laser pulse envelopes). For the case of the step-like envelope of the laser pulse, one can obtain from Eq. (13) the following equations, which define analytically the density distribution for the high-density electron beam interacting with the ultra-intense laser pulse:

$$\begin{aligned}
n(Z_{0e}, t) &= \frac{n_0(1 + p_y^2 + \kappa^2)}{2\kappa^2} \\
&\quad \times \left\{ \frac{\partial[kZ_s(Z_{0e}, \theta)]}{\partial(kZ_{0e})} + \frac{\partial[kZ_f(Z_{0e}, \theta)]}{\partial(kZ_{0e})} \right\}^{-1}_{\theta=\theta(Z_{0e},t)}, \\
\frac{\partial(kZ_s)}{\partial(kZ_{0e})} &= \frac{\partial(kZ_{in})}{\partial(kZ_{0e})} - \frac{(1 + 3a_0^2/2)\theta}{2\kappa_{in}\kappa} \\
&\quad \times \left[\left(\frac{1}{\kappa_{in}} + \frac{1}{\kappa} \right) \frac{\partial\kappa_{in}}{\partial(kZ_{0e})} - \frac{2\nu\theta}{\kappa} \right], \\
\frac{\partial(kZ_f)}{\partial(kZ_{0e})} &= -a_0^2 \frac{\sin 2\theta - 8\sin\theta}{4\kappa^3} \frac{\partial\kappa}{\partial(kZ_{0e})} \\
&\quad - a_0^2 \nu \frac{1 - cos2\theta + 16(cos\theta - 1)}{8\kappa^3} \\
&\quad \times \left[2 + \frac{3(kl - 2kZ_{0e})}{\kappa} \frac{\partial\kappa}{\partial(kZ_{0e})} \right], \\
\frac{\partial\kappa_{in}}{\partial(kZ_{0e})} &= \nu(kl - 4kZ_{0e}), \\
\frac{\partial\kappa}{\partial(kZ_{0e})} &= \frac{\partial\kappa_{in}}{\partial(kZ_{0e})} - 2\nu\theta, \\
\frac{\partial(kZ_{in})}{\partial(kZ_{0e})} &= 1 - \frac{\kappa_{in} - 1}{2\kappa_{in}} - \frac{kZ_{0e}}{2\kappa_{in}^2} \frac{\partial\kappa_{in}}{\partial(kZ_{0e})}.
\end{aligned} \tag{35}$$

4.2. PIC Simulations for the Density Distribution of the Electron Beam

To verify the predictions of the derived theory for the evolution of the dense electron beam in the super-intense laser field, the PIC simulations with the 1D version of the XOOPIC code were executed. Full details of this object-oriented fully relativistic PIC code are described by Usui *et al.* (2000). The main goal of the PIC simulations was to test the adequacy of the model, i.e., the possibility for omitting the radiation reaction force of the electrons and the importance of the supposition that the trajectories of the ESs do not cross.

In the simulations, the laser pulse had the step-like envelope with the amplitude $a_0 = 5$ and the wavelength $\lambda = 1$ μm. The length of the laser pulse was equal to 20 λ (actually, electron beam evolution will be the same for any step-like laser pulse with length greater than $\simeq 8\lambda$ for considered time of interaction of $\simeq 0.4$ ps since only eight first laser pulse cycles interact with the electron beam during this time). In Figures 4 and 5, the electron density distributions inside the laser pulse are presented for different moments of time. The electron beam before interaction had the length of $l = 10$ μm, and two different electron densities, $n_0 = 2.2 \times 10^{17}$ cm^{-3} ($\nu = 10^{-4}$) in Figure 4 and $n_0 = 2.2 \times 10^{16}$ cm^{-3} ($\nu = 10^{-5}$) in Figure 5, were utilized. In both cases, initial velocity of the electrons was equal to zero. There were 2000 (Fig. 4) or 1100 (Fig. 5) spatial grid points on the laser wavelength λ, and there were 50 macroparticles in one grid cell. Since the left sharp peaks in the density distribution are considerably higher than smooth

https://doi.org/10.1017/S0263034608000414 Published online by Cambridge University Press

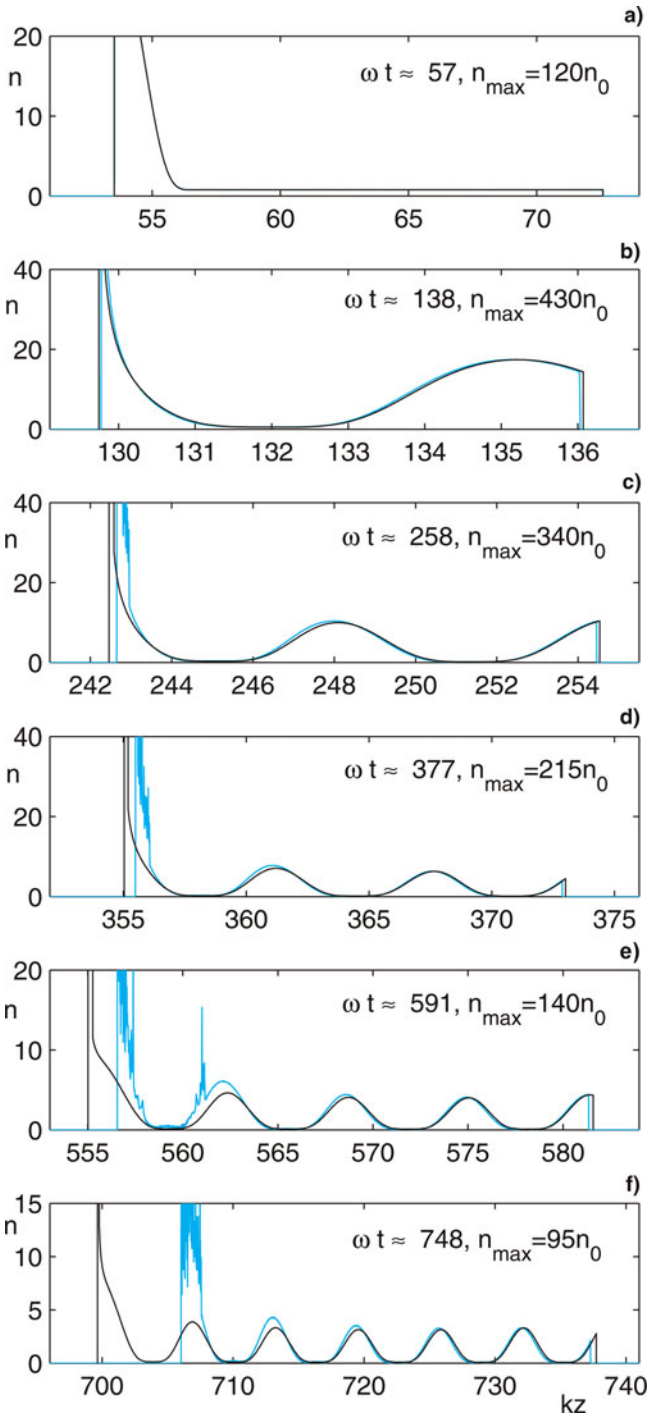

Fig. 4. (Color online) Evolution of the electron beam density distribution ($n_0 = 2.2{\cdot}10^{17}$ cm^{-3}, $\nu = 10^{-4}$) in the field of an ultra-intense laser pulse with a step-like envelope and $a_0 = 5$ [black line—theory, grey line (cyan online)—PIC simulations]. The electron density (in units of the initial density n_0) is presented for different times: $\omega t \simeq 57$, 138, 258, 377, 591, 748 for (**a**)–(**f**). Also, the maximal heights n_{max} for the sharp density peaks, obtained in the PIC simulation, are indicated for these times. Note the different vertical scales for plots (**a**)–(**f**).

peaks to the right, the values for the maximal heights $n_{\max}$ of the sharp density peaks obtained from the PIC simulation are indicated in Figure 4 also.

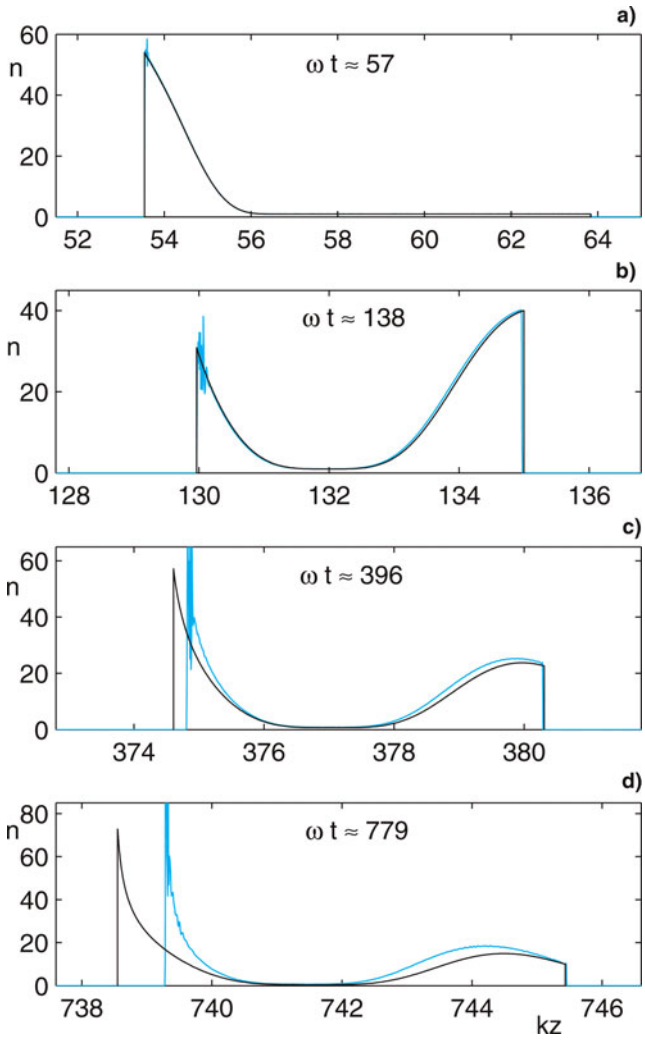

Fig. 5. (Color online) Same as in Figure 4, but for $n_0 = 2.2 \times 10^{16}$ cm^{-3}, $\nu = 10^{-5}$ [black line—theory, grey line (cyan online)—PIC simulations]. The electron density (in units of the initial density n_0) is presented for the following times: $\omega t \simeq 57$, 138, 396, 779 for (**a**)–(**d**). Note the different vertical scales for plots (a)–(f).

In the same figures, the results of calculations for the theoretical value of the electron density according to Eq. (35) are presented. Here, for every initial coordinate Z_{0e} of the ES (1000 in total), the value for parameter θ at some moment of time, t, was calculated from Eq. (5) using Eq. (13) for the value of the coordinate (the fast part Z_f of the ES's coordinate was also taken into account). Then, these values for θ for all ESs were used for plotting the electron density distribution at this moment of time, t. When the density from Eq. (35) has negative and positive values simultaneously in some points Z (many-valued function, cf. Section 4.3), then for such points, the absolute values of positive and negative parts of the density distribution were added to calculate the total density.

From these figures, one can conclude that the theory gives good agreement with the PIC simulations. There is a small difference in the positions of the sharp peaks in calculated

https://doi.org/10.1017/S0263034608000414 Published online by Cambridge University Press

and simulated density distributions. This difference oscillates with time, and its maximal values are about λ for $\nu = 10^{-4}$ and about $\lambda/10$ for $\nu = 10^{-5}$ for $\omega t \simeq 750$ (0.4 ps from the beginning of interaction). The difference in the positions of the sharp peaks can be explained by two reasons. The first reason is the physical one, i.e., the acceleration of the electrons by the radiation reaction force, which is omitted in the analytical calculations and is present in the PIC simulations. This radiation reaction force accelerates more effectively those electrons, which are incorporated into a very short bunch with length considerably smaller than the laser wavelength (Cherepenin *et al.*, 2001; Kulagin *et al.*, 2004*b*). Therefore, the position of the sharp simulation peak changes with respect to the position of the theoretical peak due to this force, while the positions of the wide diffuse simulation peaks to the right of the sharp peak are almost unchanged with respect to their theoretical positions. The other reason is numerical, i.e., not high enough accuracy of the PIC simulations. Actually, if one takes 1000 grid points on the laser wavelength λ instead of 2000 (which was used for simulations in Fig. 4) with other parameters as in Figure 4, the discrepancy in the positions of calculated and simulated sharp peaks increases. An excess noise (around sharp peaks) of the PIC simulations at large times in Figures 4 and 5 can also be explained by not high enough accuracy of the PIC simulations (to remove the noise it is necessary to increase considerably the number of spatial grid points on the laser wavelength).

4.3. Sharp Density Peak Frozen Into the Density Distribution of the Electron Beam

There is the sharp peak in the electron density distribution at the left end of the electron beam, where the laser pulse strikes first (cf. Figs. 4 and 5). Since the position of this peak does not change with time with respect to the electron beam, it can be considered as frozen into the density distribution. All other peaks are the peaks of the density wave inside the electron beam (Kulagin *et al.*, 2006*a*) defined by the factor γ, and they change their position with time. The position of the frozen peak is defined by the factor $\partial[kZ(Z_{0e}, \theta)]/\partial(kZ_{0e})$ in the expression for the density distribution (34), more precisely, by the points, where this factor is close (or equal) to zero. To investigate the conditions for the appearance of the frozen density peak, let us consider more closely Eq. (35) for the density distribution in the field of the laser pulse with the step-like envelope. The height of the density peak changes slowly with time so the fast part kZ_f of the coordinate of ESs can be disregarded, and only the slow part kZ_s should be analyzed. Then, from the last equation of the system (35), one can estimate that $\partial(kZ_{in})/\partial(kZ_{0e}) \simeq 1$ for reasonable parameters of the electron beam, and the only term, which can give the divergence of n, is the term proportional to $\partial\kappa_{in}/\partial(kZ_{0e})$ in $\partial(kZ_s)/\partial(kZ_{0e})$. This means that, for the electron beams without initial modulation of velocity, there will be no frozen peak in the density distribution. For the dense electron beams, such a modulation is provided by the space-charge (Coulomb) forces in the beam. Also, since initial velocity modulation is strongly dependent on the initial conditions of the problem, the parameters of the frozen density peak will be varied for different initial conditions, e.g., will depend on the presence of focusing forces for the electron beam, etc. The parameters of the laser pulse front also influence on the appearance and characteristics of the sharp density peak.

From the physical point of view, the equality of the derivative $d[kZ(Z_{0e}, t)]/d(kZ_{0e})$ to zero, which causes the divergence of the density, means only the crossing of the trajectories of the ESs, i.e., after some time, two ESs with different initial coordinates arrive at the same point z_{cr}. This, of course, does not mean any inconsistency in the approach since the surface charge density is limited for any layer with finite length around z_{cr} (the infinity is "integrable"). On the other hand, our model and exact solutions (8) are based on the assumption that there are no crossings of the trajectories of ESs during evolution of the electron beam in the super-intense laser pulse. If such crossings occur then the Coulomb forces for the ESs with the crossed trajectories are calculated inaccurately, and the motion of these ESs is reproduced only approximately by the model. So, strictly speaking, Eq. (8) are valid only for such parameters of the electron beam and the laser pulse, for which there are no divergence of the electron beam density. However, if the number of crossings is not large (only small part of the trajectories of the ESs crosses), then Eq. (8) can be considered as the approximate solutions for those ESs, which suffer the crossings of the trajectories, and as exact solutions for the other ESs.

To derive approximate conditions for the appearance of the frozen density peak and the crossings of the trajectories, let us suppose that $\kappa \simeq \kappa_{in} \simeq 1$, that is, reasonable for not very large values of θ. Then, from the second equation of the system (35), one has

$$\frac{\partial(kZ)}{\partial(kZ_{0e})} \simeq 1 - (1 + 3a_0^2/2)\theta(\nu kl - 4\nu kZ_{0e} - \nu\theta). \qquad (36)$$

The electron beam density will be infinite in the points where this partial derivative is equal to zero. Then, from quadratic equation for θ, one can estimate two possible solutions

$$\theta = \frac{1}{2}\{kl - 4kZ_{0e} \pm \sqrt{(kl - 4kZ_{0e})^2 - 4/[\nu(1 + 3a_0^2/2)]}\}. \qquad (37)$$

The frozen density peak can appear only during interaction of electromagnetic wave with the dense electron beam; when the beam evolves freely under the action of the Coulomb forces only, the density distribution has no sharp peaks. So for the parameter θ, only positive values are possible. Then, from Eq. (37), one can conclude that $kZ_{0e} < kl/4$.

https://doi.org/10.1017/S0263034608000414 Published online by Cambridge University Press

To have real solutions, the determinant should be non-negative, that gives together with the previous condition the following inequality $kZ_{0e} \le kl/4 - [2\sqrt{\nu(1+3a_0^2/2)}]^{-1}$, and the divergence in the density distribution of the electron beam is possible only for $\nu(kl)^2(1+3a_0^2/2) = \alpha kl(1+3a_0^2/2) \ge 4$.

The crossings of the trajectories begin first for the ESs with initial coordinates around $Z_{0e} \simeq 0$ (the left ESs, which are touched first by the laser pulse front). This occurs at

$$\theta_{cr1} = [(1+3a_0^2/2)\alpha]^{-1}, \quad \omega t_{cr1} \approx (2\alpha)^{-1}, \tag{38}$$

where $(1+3a_0^2/2)\alpha kl \gg 4$ is supposed, and for the transition from θ to ωt, Eq. (14) is utilized with the same assumptions that were used for deriving Eq. (36). Then, at time

$$\theta_{cr2} = kl, \quad \omega t_{cr2} \approx 3kla_0^2/4, \tag{39}$$

the crossings of the trajectories for these ESs will disappear (however, the frozen density peak will die only when the condition $\theta \gg \theta_{cr2} = kl$ is fulfilled for the left ESs). The value (39) for θ_{cr2} is less accurate than Eq. (38) for θ_{cr1} since, for such a large time, approximation of κ by unity can be invalid.

The initial coordinate Z_{0e} of the last (the most right) ES, which still suffer the crossings of the trajectories, is defined by expression

$$kZ_{0max} = kl/4 - \left[2\sqrt{\nu(1+3a_0^2/2)}\right]^{-1}. \tag{40}$$

The value

$$kZ_{0_{max}}/kl = \frac{1}{4} - \frac{1}{2\sqrt{\alpha kl(1+3a_0^2/2)}}, \tag{41}$$

gives just the part of the ESs, which outstrips the neighboring ESs. So in the worst case, this part is about 0.25. The ES with the initial coordinate kZ_{0max} will suffer the crossing of the trajectories, or, more exactly, touching of the trajectories as long as $\theta_{cr1} = \theta_{cr2}$, at time

$$\theta_t = \left[\sqrt{(1+3a_0^2/2)\nu}\right]^{-1}, \quad \omega t_t \approx \sqrt{\frac{3a_0^2}{8\nu}}. \tag{42}$$

It can be checked easily that $\omega t_{cr1} \le \omega t_t \le \omega t_{cr2}$ for all parameters of the electron beam and the laser pulse.

Let us now make some estimates for the simulated electron beams with $\nu = 10^{-4}$ and $\nu = 10^{-5}$. For the $\nu = 10^{-5}$ case, $\alpha kl(1+3a_0^2/2) \simeq 1.5 < 4$, and there are no crossings of the trajectories and divergence of the density distribution. However, the frozen peak still exists, because the value for $\alpha kl(1+3a_0^2/2)$ here is comparable with 4. For the $\nu = 10^{-4}$ case, $\alpha kl(1+3a_0^2/2) \simeq 15 \gg 4$, and there are the crossings of the trajectories and the divergence of the density distribution. The first crossing takes place according to the estimate (38) at $\omega t_{cr1} \simeq 80$, this value from numerical solutions of Eq. (6) is equal to 88. So in Figure 4a, there are no crossings of the trajectories. The crossings of the trajectories disappear at $\omega t_{cr2} \simeq 1180$ (numerical value is about 950), and the time for the touching of the trajectories by the ES with the initial coordinate $kZ_{0max} \simeq 0.12kl$ is $\omega t_t \simeq 310$ (numeric value is about 320). Therefore, in Fig. 4b to 4f, the trajectories are crossed near the left end of the electron beam, and the analytic expression for the electron beam density has the divergence here. However, from the calculations with the self-consistent MATLAB code EXACT (Cherepenin *et al.*, 2001; Kulagin *et al.*, 2004*b*, 2007*b*), the results for which are presented in Figure 2a, one can conclude that all the ESs, which suffer the crossings of the trajectories, stay within the distance of $\lambda/10$ near the sharp density peak. In this case, the value, obtained from the PIC simulation for the maximal height η_{max} of the sharp density peak, characterizes indirectly the part of the ESs with the crossed trajectories. So the estimates (38), (39), and (42) provide the reasonable approximations to the characteristic time points of the evolution for the frozen density peak.

5. DISCUSSION OF RESULTS AND CONCLUSIONS

The theory, presented above for the interaction of the high-density electron beam with the super-intense laser pulse, shows that there are two conditions, which define the characteristics for the evolution of the electron beam. The first condition is applicable to the initial period of motion of the electrons in the beam, when the laser pulse still have not reached them. This condition defines whether the space-charge (Coulomb) forces do or do not play a determinative role in the evolution of the electrons during this period. More exactly, when $\alpha kl = 2\pi^2 l^2/\lambda_p^2 \ll 1$, where $\lambda_p = 2\pi c/\omega_p$, or, equivalently, $l \ll \lambda_p/(\pi\sqrt{2})$, the Coulomb forces do not change significantly the initial coordinates of the electrons before the laser pulse reaches them, so the electron beam can be considered as a low-density beam (with regard to this particular problem of interaction). In the opposite case, when $\alpha kl \lesssim 1$, the Coulomb forces considerably change the initial coordinates of the electrons during the time, required for the laser pulse to reach them (Fig. 2a).

The second condition deals with the crossings of the electron trajectories resulting in the infinite analytical value for the electron density in the beam. This occurs when $\alpha kl(1+3a_0^2/2) \ge 4$. When the crossings of the trajectories start, some electrons in the electron beam become to participate in the multi-stream motion. The crossings of the trajectories result in appearance of the sharp high-density peak frozen into the density distribution at the side of the electron beam, which is touched first by the laser pulse front. The characteristics of this sharp density peak strongly depend on the initial conditions of the motion for the electrons, i.e., on initial modulation of velocity of the electrons, on the presence of the focusing forces, etc., and on the parameters of the laser pulse front.

https://doi.org/10.1017/S0263034608000414 Published online by Cambridge University Press

It is necessary to note that both conditions depend not only on the initial density of the electron beam, but also on its length. So electron beams with relatively low density but large length can demonstrate the described effects. The second condition depends also on the amplitude of the laser pulse, therefore, for high enough amplitudes, the sharp peak of the density can appear in the low-density electron beams.

These sharp peaks in the electron beams can be effectively used as attosecond electron beams in different applications. Thus, estimates based on Figures 4 and 5 give the length of this peaks on the level of several nanometers, which results in the duration of about several attoseconds. Also, these sharp peaks can be used for the generation of coherent X-ray radiation, required in many applications (Barbara *et al.*, 1994; Crowell *et al.*, 2004).

If the laser pulse will have a smooth front, then the transverse momentum of the electrons will be determined by an expression different from Eq. (10). However, all parameters for the electron beam evolution can be easily recalculated for this case with the help of Eq. (8). Qualitatively, the main difference for the smooth front will be the other distance between the layers in the multilayer configuration - $\lambda/2$ instead of λ for the sharp front (Kulagin *et al.*, 2006*a*, 2006*b*). Spread of initial parameters for the electrons in the beam due to, e.g., thermal effects, can increase the sharp peak width. However, for high enough laser pulse amplitudes and not very large initial electron temperatures, this effect will be not prominent, at least, in the beginning of interaction. Note that the microbunching structure of the electron beam is extremely stable and does not depend on the thermal properties of the electrons since the microbunching is defined only by the distribution of the electromagnetic field in space.

Let us estimate at last some practical laser parameters required for realization of considered scheme for high-density electron beam preprocessing. If the longitudinal dimensions of the electron medium is about 10 μm (that is inherent for electron beams from laser-plasma accelerators, and can be achieved for focused ordinary electron beams in the scheme of perpendicular propagation of electron and accelerating laser beams) then the laser spot should be not less than 20 μm. For $a_0 = 5$, this requires the laser power of 50–100 TW that is easily accessible in experiment.

In summary, the evolution of the high-density electron beam in the field of the super-intense laser pulse was considered. The theory for the interaction was developed, and the exact solutions for the equations of motion of the electrons were found. The main differences of this high-density electron beam case from the low-density case (Kulagin et al., 2006*a*, 2006*b*) are the slow increase of the electron beam length in time after initial compression of the beam and the appearance of the sharp density peak frozen into the density distribution of the electron beam. Characteristic parameters for the evolution of the electron beam were calculated by an example of a step-like envelope of the laser pulse. Comparison with the 1D PIC simulations shows that, for $\alpha kl(1 + 3a_0^2/2) < 4$ the theory correctly describes the density of the electron beam inside the super-intense laser pulse. In the opposite case, $\alpha kl(1 + 3a_0^2/2) \geq 4$, the theory adequately describes the smooth part of the density distribution, where the trajectories of the electrons do not cross and approximately describe the density distribution around the sharp density peak, where the crossings of the electron trajectories exist (multi-stream region).

ACKNOWLEDGMENTS

This work was supported by the Ministry of Knowledge and Economy of Korea through the Ultrashort Quantum Beam Facility Program and the GIST Top Brand Project "Photonics 2020," and by the RFBR project 05-02-17297-a.

REFERENCES

Baeva, T., Gordienko, S. & Pukhov, A. (2007). Relativistic plasma control for single attosecond pulse generation: Theory, simulations, and structure of the pulse. *Laser Part. Beams* **25**, 339–346.

Barbara, P.F., Knox, W.H., Mourou, G.A. and Zewail, A.H., eds. (1994). *Ultrafast Phenomena IX*, Berlin: Springer-Verlag.

Brau, C.A. (1990). *Free-Electron Lasers*. San Diego: Academic.

Canova, F., Flacco, A., Canova, L., Clady, R., Chambaret, J.-P., Ple, F., Pittman, M., Planchon, T.A., Silva, M., Benocci, R., Lucchini, G., Batani, D., Lavergne, E., Dovillaire, G. & Levecq, X. (2007). Efficient aberrations pre-compensation and wavefront correction with a deformable mirror in the middle of a petawatt-class CPA laser system. *Laser Part. Beams* **25**, 649–655.

Cherepenin, V.A., Il'in, A.S. & Kulagin, V.V. (2001). Acceleration of dense electron bunches at the front of a high-power electromagnetic wave. *Fiz. Plazmy* **27**, 1111–1120.

Cherepenin, V.A. & Kulagin, V.V. (2004). Dynamics and radiation of thin foil in the field of super-intense laser pulse. *Phys. Lett.* **321A**, 103–110.

Crowell, R.A., Gosztola, D.J., Shkrob, I.A., Oulianov, D.A., Jonah, C.D. & Rajh, T. (2004). Fundamentals of radiation chemistry. *Radiat. Phys. Chem.* **70**, 501–509.

Danson, C.N., Brummitt, P.A., Clarke, R.J., Collier, I., Fell, B., Frackiewicz, A.J., Hawkes, S., Hernandez-Gomez, C., Holligan, P., Hutchinson, M.H.R., Kidd, A., Lester, W.J., Musgrave, I.O., Neely, D., Neville, D.R., Norreys, P.A., Pepler, D.A., Reason, C., Shaikh, W., Winstone, T.B., Wyatt, R.W.W. & Wyborn, B.E. (2005). Vulcan petawatt: Design, operation and interactions at 5×10^{20} Wcm^{-2}. *Laser Part. Beams* **23**, 87–93.

Esarey, E., Ride, S.K. & Sprangle, P. (1993). Nonlinear Thomson scattering of intense laser pulses from beams and plasmas. *Phys. Rev. E*, **48**, 3003–3021.

Faure, J., Glinec, Y., Pukhov, A., Kiselev, S., Gordienko, S., Lefebvre, E., Rousseau, J.-P., Burgy, F. & Malka, V. (2004). A laser-plasma accelerator producing monoenergetic electron beams. *Nature* **431**, 541–544.

Flippo, K., Hegelich, B.M., Albright, B.J., Yin, L., Gautier, D.C., Letzring, S., Schollmeier, M., Schreiber, J., Schulze, R. &

Fernandez, J.C. (2007). Laser-driven ion accelerators: Spectral control, monoenergetic ions and new acceleration mechanisms. *Laser Part. Beams* **25**, 3–8.

Fubiani, G., Qiang, J., Esarey, E., Leemans, W.P. & Dugan, G. (2006). Space charge modeling of dense electron beams with large energy spreads . *Phys. Rev. ST Accel. Beams* **9**, 064402.

Geddes, C.G.R., Toth, Cs., van Tilborg, J., Esarey, E., Schroeder, C.B., Bruhwiler, D., Nieter, C., Cary, J. & Leemans, W.P. (2004). High-quality electron beams from a laser wakefield accelerator using plasma-channel guiding. *Nature* **431**, 538–541.

Gupta, D.N. & Suk, H. (2007). Electron acceleration to high energy by using two chirped lasers. *Laser Part. Beams* **25**, 31–36.

Hafz, N.M, Choi, I.W., Sung J.H., Kim, H.T., Hong, K.-H., Jeong, T.M., Yu, T.J., Kulagin, V., Suk, H., Noh, Y.-C., Ko, D.-K. & Lee, J. (2007). Dependence of the electron beam parameters on the stability of laser propagation in a laser wakefield accelerator. *Appl. Phys. Lett*. **90**, 151501.

Il'in, A.S., Kulagin, V.V. & Cherepenin, V.A. (1999). Radiation effects in the electron sheet model. *Radiotekh. Elektron*. **44**, 389–400.

Kalashnikov, M., Osvay, K. & Sandner, W. (2007). High-power Ti:Sapphire lasers: Temporal contrast and spectral narrowing. *Laser Part. Beams* **25**, 219–223.

Karmakar, A. & Pukhov, A. (2007). Collimated attosecond GeV electron bunches from ionization of high-Z material by radially polarized ultra-relativistic laser pulses. *Laser Part. Beams* **25**, 371–377.

Koyama, K., Adachi, M., Miura, E., Kato, S., Masuda, S., Watanabe, T., Ogata, A. & Tanimoto, M. (2006). Monoenergetic electron beam generation from a laser-plasma accelerator. *Laser Part. Beams* **24**, 95–100.

Kulagin, V.V., Cherepenin, V.A. & Suk, H. (2004*a*). Generation of relativistic electron mirrors and frequency upconversion in laser-plasma interactions. *Appl. Phys. Lett*. **85**, 3322–3324.

Kulagin, V.V., Cherepenin, V.A. & Suk, H. (2004*b*). Compression and acceleration of dense electron bunches by ultraintense laser pulses with sharp rising edge. *Phys. Plasmas* **11**, 5239–5249.

Kulagin, V.V., Cherepenin, V.A., Hur, M.S. & Suk, H. (2006*a*). Compression and microbunching of electron beams by ultra-intense laser pulses. *Phys. Lett*. **353A**, 505–511.

Kulagin, V.V., Hur, M.S. & Suk, H. (2006*b*). Bunching of electron beams by ultra-relativistic laser pulses. *J. Korean Phys. Soc*. **48**, 747–754.

Kulagin, V.V., Cherepenin, V.A., Hur, M.S. & Suk, H. (2007*a*). Theoretical investigation of controlled generation of a dense attosecond relativistic electron bunch from the interaction of an ultrashort laser pulse with a nanofilm. *Phys. Rev. Lett.*, **99**, 124801.

Kulagin, V.V., Cherepenin, V.A., Hur, M.S. & Suk, H. (2007*b*). Flying mirror model for interaction of a super-intense nonadiabatic laser pulse with a thin plasma layer: Dynamics of electrons in a linearly polarized external field. *Phys. Plasmas* **11**, 113101.

Landau, L.D. & Lifshitz, E.M. (1975) *The Classical Theory of Fields*. Oxford: Pergamon.

Lapostolle, P., Lombardi, A.M., Tanke, E., Valero, S., Garnett, R.W. & Wangler, T.P. (1996). A modified space charge routine for high intensity bunched beams. *Nucl. Instrum. Methods Phys. Res., Sect. A* **379**, 21–40.

Lifschitz, A.F., Faure, J., Glinec, Y., Malka, V. & Mora, P. (2006). Proposed scheme for compact GeV laser plasma accelerator. *Laser Part. Beams* **24**, 255–259.

Mangles, S.P.D., Murphy, C.D., Najmudin, Z., Thomas, A.G.R., Collier, J.L., Dangor, A.E., Divall, E.J., Foster, P.S., Gallacher, J.G., Hooker, C.J., Jaroszynski, D.A., Langley, A.J., Mori, W.B., Norreys, P.A., Tsung, F.S., Viskup, R., Walton, B.R. & Krushelnick, K. (2004). Monoenergetic beams of relativistic electrons from intense laser–plasma interactions. *Nature* **431**, 535–538.

Marshall, T.C. (1985). *Free-Electron Lasers*. New York: McMillan.

Neumayer, P., Bock, R., Borneis, S., Brambrink, E., Brand, H., Caird, J., Campbell, E.M., Gaul, E., Goette, S., Haefner, C., Hahn, T., Heuck, H.M., Hoffmann, D.H.H., Javorkova, D., Kluge, H.J., Kuehl, T., Kunzer, S., Merz, T., Onkels, E., Perry, M.D., Reemts, D., Roth, M., Samek, S., Schaumann, G., Schrader, F., Seelig, W., Tauschwitz, A., Thiel, R., Ursescu, D,. Wiewior, P., Wittrock, U. & Zielbauer, B. (2005). Status of PHELIX laser and first experiments. *Laser Part. Beams* **23**, 385–389.

Reiser, M. (1994). *Theory and Design of Charged Particle Beams*. New York: Wiley.

Reitsma, A.J.W., Goloviznin, V.V., Kamp, L.P.J. & Schep, T.J. (2001). Simulation of laser wakefield acceleration of an ultrashort electron bunch. *Phys. Rev. E* **63**, 046502.

Sakai, K., Miyazaki, S., Kawata, S., Hasumi, S. & Kikuchi, T. (2006). High-energy-density attosecond electron beam production by intense short-pulse laser with a plasma separator. *Laser Part. Beams* **24**, 321–327.

Saldin, E.L., Schneidmiller, E.A. & Yurkov, M.V. (1999). *The Physics of Free Electron Lasers*. Berlin: Springer-Verlag.

Saldin, E.L., Schneidmiller, E.A. & Yurkov, M.V. (2008). Coherence properties of the radiation from X-ray free electron laser. *Opt. Comm*. **281**, 1179–1188.

Umstadter, D., Kim, J.K. & Dodd, E. (1996). Laser injection of ultrashort electron pulses into wakefield plasma waves. *Phys. Rev. Lett*. **76**, 2073–2076.

Usui, H., Verboncoeur, J.P. & Birdsall, C.K. (2000). Development of 1D object-oriented particle-in-cell code (1d-XOOPIC). *IEICE Trans. Electron*. **E83C**, 989–992.

Vshivkov, V.A., Naumova, N.M., Pegoraro, F. & Bulanov, S.V. (1998). Nonlinear electrodynamics of the interaction of ultra-intense laser pulses with a thin foil. *Phys. Plasmas*, 2727–2741.

Wangler, T.P. (1998). *RF Linear Accelerators*. New York: Wiley, 270–272.

Zhou, C.T., Yu, M.Y. & He, X.T. (2007). Electron acceleration by high current-density relativistic electron bunch in plasmas. *Laser Part. Beams* **25**, 313–319.

Zvorykin, V.D., Didenko, N.V., Ionin, A.A., Kholin, I.V., Konyashchenko, A.V., Krokhin, O.N., Levchenko, A.O., Mavritskii, A.O., Mesyats, G.A., Molchanov, A.G., Rogulev, M.A., Seleznev, L.V., Sinitsyn, D.V., Tenyakov, S.Y., Ustinovskii, N.N. & Zayarnyi, D.A. (2007). GARPUN-MTW: A hybrid Ti: Sapphire/KrF laser facility for simultaneous amplification of subpicosecond/nanosecond pulses relevant to fast-ignition ICF concept. *Laser Part. Beams* **25**, 435–451.